Electric fields, forces, and modification of the tunnel barrier during field electron emission and field evaporation from single-wall carbon nanotubes

Vladimir Pimonov, Federico Panciera, Goulven Rouille, Catherine Weng, Sorin Perisanu, Costel Sorin Cojocaru, Haifa Taoum, Chen Wei, Salvador Barranco Carceles, Victor Verdugo-Gutiérrez, et al.

Journal of Vacuum Science & Technology B

Electric fields, forces and modification of the tunnel barrier during field electron emission and field evaporation from single-wall carbon nanotubes

Vladimir Pimonov,[1] Federico Panciera,[2] Goulven Rouille,[1] Catherine Weng,[1] Sorin Perisanu,[1] Costel Sorin Cojocaru,[3] Haifa Taoum,[3] Chen Wei,[2] Salvador Barranco Carceles,[1] Victor A. Verdugo-Gutiérrez,[2] Ilias Aguili,[1] Jean Francois Sivignon,[1] Nicholas Blanchard,[1] Pierre Legagneux,[4] Stephen Thomas Purcell,[1] Anthony Ayari,[1] and Pascal Vincent[1]

[1)]*Univ Lyon, Univ Claude Bernard Lyon 1, CNRS, Institut Lumiere Matiere, F-69622, Villeurbanne, France.*

[2)]*University of Paris-Saclay, CNRS, Centre for Nanoscience and Nanotechnology, 91120 Palaiseau, France.*

[3)]*Laboratory of Physics of Interfaces and Thin Films, UMR CNRS 7647, Ecole Polytechnique, IP-Paris, 91228 Palaiseau, France.*

[4)]*Thales Research and Technology, Palaiseau, France.*

(*Electronic mail: pascal.vincent@univ-lyon1.fr)

(Dated: 26 June 2025)

In this paper we theoretically and experimentally investigate the specificities of single-walled carbon nanotubes (SWNTs) for field electron emission (FE) and field ion evaporation (FI). For FE the small radii of curvature of these nanotubes lead to a significant widening of the tunnel barrier and thus for a given emission current the fields at the surface of the SWNTs are significantly higher than commonly observed in standard large radius FE. For currents in the μA range for example, fields ranging from 7-8 V/nm for large nanotubes to 17-18 V/nm for the thinnest are required. These strong fields in turn have repercussions on FI and electrostatic forces. The electric fields and longitudinal electrostatic forces during FE and FI as a function of nanotube radius are presented. The evolution of the nanotube during field evaporation was also studied in an environmental transmission electron microscope as a function of field strength and polarity. A strong dissymmetry between positive and negative polarity is observed. For negative polarity the nanotubes can gradually shorten as the voltage is increased whereas in positive polarity, they are almost systematically torn off before apex evaporation occurs. A model to explain this dissymmetry for our samples is presented. These results can be used to optimize nanotube cathode geometries.

I. INTRODUCTION

In the experimental literature, estimates of electric fields at the apex of single-walled carbon nanotubes (SWNTs) during field electron emission (FE) vary widely. Dean *et al.*[1] estimate the maximum fields in their studies at about 4.5 V/nm for currents of several hundred nA, similar to Saito *et al.*[2] for somewhat different currents. On the other hand, Edgecombe *et al.*, using the I(V) curve and the electron total energy distribution, TED, estimate a field of 13.5 V/nm for a current of 105 nA[3]. Furthermore Pascale-Hamri *et al.*[4] using Coulomb oscillations during FE, estimate a field of 11 V/nm for a current of 10 pA for a triangular barrier. The gap is striking between 4.5 V/nm for near μA and 11 V/nm for 10 pA.

Theoretically, when the radius of curvature of an emitter is sufficiently small, i.e. on the scale of the 1-2 nm range of the tunneling barrier itself, the surface potential is significantly curved and the electric field weakened as a function of distance from the emitter[5–8]. As a consequence the tunneling barrier is wider and emission currents are lower than those predicted by the surface field and standard emission theory. This is quantified below in part II. Higher surface fields than the standard 3-7 V/nm are therefore needed to compensate the lowered emission for the extreme low radii SWNTs. This has not yet been well explored in the experimental literature for the extreme low radii SWNTs which are an important class of cold electron cathode. An improved determination of these surface and near surface fields is crucial as they govern numerous phenomena such as field electron emission, field ion evaporation (FI), electrostatic forces and stresses.

Another aspect is the observation of FI from SWNTs and multiwall nanotubes (MWNTs) during field emission. Note that, in principle, FE depends on the whole barrier while FI would depend more closely on the surface field. A thermally assisted field evaporation process has been proposed[1] where temperatures are increased by FE current induced heating of the nanotubes. The questions are, what are the fields associated with this evaporation and is invoking a temperature increase necessary ?

The aim of this article is to clarify a number of points concerning SWNTs, and carbon nanotubes more generally, such as the fields required for field emission as a function of nanotube radius, the evaporation mechanisms as a function of field strength and polarity, and the estimation of electric field induced forces and stresses to better understand nanotube destruction mechanisms. For this purpose simulations using classical electrostatics and tunneling theory are first carried out, followed by experimental comparisons of FI under negative and positive polarity. These experiments were performed in an Environmental Transmission Electron Microscope (ETEM) using a recently published electric field directed synthesis (EFDS) technique[9,10]. This makes it possible to grow *in situ* principally straight SWNTs under positive or negative polarity and to follow the evolution of these nanotubes as the applied voltage is varied. There is a marked dissymmetry between the two polarities, which we explore.

In summary, the results of our simulations on the widening of the tunneling barrier are first presented. In the second part, the experimental and theoretical results obtained on field evaporation in positive and negative polarities are discussed; then our experiments of *in situ* evaporation in ETEM are presented. The forces and stresses generated by high fields are discussed in a third section. Finally, we discuss the consequences of our observations and propose a scenario to explain the significant dissymmetry observed in our case.

II. FIELD, POTENTIAL BARRIER AND EMISSION CURRENT

Electrostatic simulations were performed with COMSOL with the nanotube approximated as a metallic cylinder terminated by a perfect hemisphere perpendicular to the electrodes in an infinite capacitor with a gap of 2 μm. These parameters have been chosen to be close to those of the samples we have previously studied in ETEM, where the two electrodes with a thickness of 4 μm are separated by a gap of 2 μm[9,10]. Experimentally, the complete environment (objective lens pole pieces, the other parts of sample, screening of nearby nanotubes, etc.) tends to slightly reduce the field enhancement factor. Furthermore, semiconductor SWNTs (sc-SWNTs) are mostly small bandgap semiconductors, and since growth and FE experiments were performed at $\approx$ 1000 K, they are considered electrically equivalent to metallic SWNTs (m-SWNTs).

Simulation by density functional theory (DFT) may seem more relevant for these nanometric objects. However, despite some very interesting recent advances[11,12], these approaches still have major limitations, for example with regard to the handling of strong fields, the very limited size of the system due to the very low number of atoms that can be modeled and the connection with electronic emission. Moreover, recent works[13–16] have shown that the field distributions predicted by classical electrostatic models align well with induced-charge distributions calculated using DFT, thereby corroborating our simulations. This said, we limited our simulations mostly to radii larger than 0.5 nm.

Figure 1 presents the simulations for the surface potential for a nanotube of radius r = 1 nm, length L = 1 μm (end of the tube in the middle of the gap) and a voltage difference of 20 V (electric field in the gap, F_G = 10 V/μm). Figure 1a) shows the evolution of the electric field, F(z), along the nanotube axis as a function of the distance from the apex of the hemisphere. The surface field F(0) is 6.06 V/nm and decreases rapidly with distance being only 1.64 V/nm at 1 nm, almost 4 times less than at the surface. The classical field enhancement factor γ is defined by $\gamma = F(0)/V$ = 303 10^6 m^{-1} and using $F(0) = \beta F_G$ gives β = 606 close to the result obtained by the analytical formula from Edgcombe and Valdrè[17,18] for a counter electrode at infinity ($\beta = 1.2(2.15 + L/r)^{0.9} = 602.6$). There is agreement for the F(0) predicted by COMSOL and the formula, but unlike a larger tube, e.g. over 20 nm, where the field would be almost constant over the several nanometres of the tunnel barrier, here it decreases sharply even over the first nanometer.

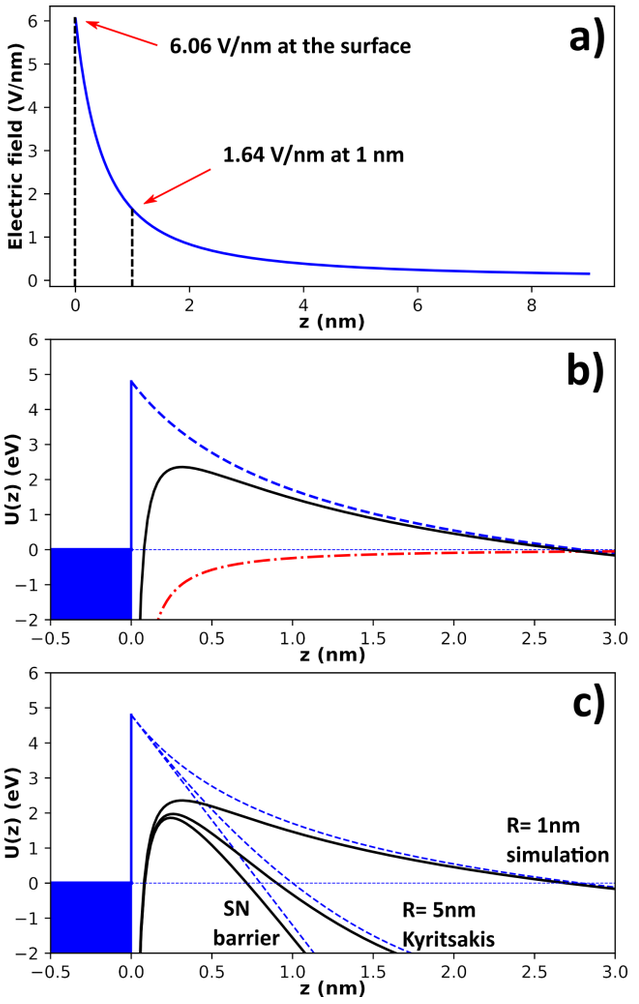

FIG. 1. a) Variation of the electric field close to the nanotube surface simulated in COMSOL for a radius of 1 nm. At the surface of the tube the field is 6.06 V/nm but is only 1.64 V/nm at 1 nm from the apex and 0.6 V/nm at 3 nm where in b) the potential crosses the Fermi level. b) Potential barrier at 0-3 nm from the surface of a nanotube of radius 1 nm obtained from the potentials calculated using COMSOL (work function 4.8 eV). c) Comparison of different barriers with the same surface field of 6 V/nm according to the chosen configuration: planar, ellipsoid (radius of curvature 5 nm) and nanotube of radius 1 nm.

Two field emission models were tested to investigate the influence of the barrier shape on the effective emission areas (total current divided by the current density at the apex) : one “Fowler-Nordheim”, or "FN", model with a triangular barrier (see complete equation in[19]) and one “Schottky-Nordheim”, or "SN" model with an image potential (see[20]). From the fields calculated on the surface, the emitted currents by the different spherical zones of the hemisphere have been calculated and integrated to obtain the total emission current. In all our calculations, the nanotube work function is set to 4.8 eV, an average of the different values found in the literature[21–24]. Thus, for the same field of 6.06 V/nm at the apex, a current of 0.177 nA is obtained from the FN model[19], while the SN

model[20] yields a current of 34.3 nA. Interestingly, although the barrier shapes and the two currents are very different, the effective areas are almost identical for the two models, 2.20 and 2.12 nm^2. In the following, the values of these effective areas are used in our WKB approach.

Now consider the modifications of the potential barrier due to the small radii of curvature[5–8]. For example, Kyritsakis *et al.*[6] have studied the effects of decreasing the local radius of curvature on ellipsoids and developed the surface potential to second order. They give the potential energy barrier seen by an electron at the Fermi level as:

$$U(z) = \phi - eFz - \frac{e^2}{16\pi\varepsilon_0}\frac{1}{z(1+z/2R)} + \frac{eF}{R}z^2 \qquad (1)$$

where ϕ is the work function, $-eFz$ is the classical linear variation of the potential, $\frac{e^2}{16\pi\varepsilon_0}\frac{1}{z(1+z/2R)}$ is the image potential for a sphere of radius R and $\frac{eF}{R}z^2$ is the non-linear variation of the potential due to the small radius of curvature of the emitter leading to the widening of the tunnel barrier and reduction in the current. They give the range of validity of their model as between 5 and 20 nm. For larger radii the difference with the classical model becomes negligible, and for smaller radii, the second-order expansion becomes insufficient. In our case, a radius of 1 nm is expected to produce even more pronounced effects. Atomic scale emitters such as graphene are assumed outside the scope of these classical calculations[25].

Figure 1b) presents the simulated evolution of the potential along the nanotube axis (blue dashed curve, 20 V applied) where, as expected, a strong non-linearity is observed. The image potential determined for a sphere of radius 1 nm is represented by the red dash-dotted curve and the resulting potential barrier corresponds to the black solid curve. The rapid decay of the field thus accompanies a considerable broadening of the potential barrier. To compare this barrier widening, Fig. 1c) presents 3 different configurations with the same F(0) = 6 V/nm and ϕ = 4.8 eV. The first is the classical planar SN model with constant field and planar image potential, where the tunnel barrier width is 0.72 nm for electrons at the Fermi level. The second model is from Kyritsakis *et al.*[6], equation 1, with a radius of 5 nm. We observe essentially a small broadening with a barrier width of 0.9 nm. The last model corresponds to our simulations, Fig. 1b), where a significant broadening of the barrier width up to 2.69 nm from the surface is observed. Thus, the field at the surface and the enhancement factor are no longer simply inversely proportional to the width of the barrier as in the classically used planar models. A large part of the results in this article are a consequence of this substantial barrier broadening.

To numerically calculate the FE current taking into account this enlarged barrier a 1D WKB approach is used combined with a free electrons model in the nanotube. The effective emission areas determined previously were used to obtain the emission current. For F(0) = 6.06 V/nm the FE current is calculated to be the extremely low value of 8.4 x 10^{-9} nA. Note that since the potential varies non-linearly, so does the width of the barrier as a function of the applied voltage, leading to a FE current that varies even more rapidly than in the conventional FN tunneling.

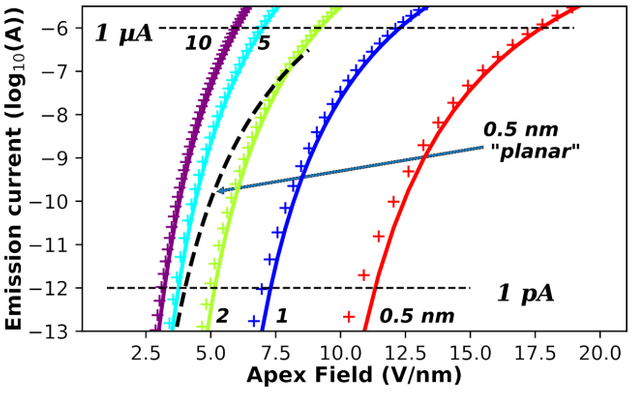

FIG. 2. Calculated FE current using simulated potential barrier as a function of the electric field at the apex for different nanotube radii: 10, 5, 2, 1 and 0.5 nm and for a length of 1μm. The solid curves and crosses correspond to 300 K and 1000 K respectively. For larger tubes we obtain the classical fields required for FE (between 3 and 7 V/nm). As the radius decreases (and the tunnel barrier widens), the electric field at the surface required increases sharply. For the thinnest tube simulated, the field can reach more than 17 V/nm for an emission current of 1 μA. For comparison the curve extrapolated using planar models for 0.5 nm is plotted as the dashed black curve (see text).

Fig. 2 depicts the calculated FE currents as a function of the electric field at the nanotube apex for different nanotube radii. The tube length is held constant at 1 μm with the different radii corresponding to r = 0.5, 1, 2, 5 and 10 nm. The solid curves correspond to a temperature of 300 K while the crosses correspond to 1000 K, which is the temperature used during growth and FE/FI experiments. Obviously, for the largest radii, this would correspond to small multiwall nanotubes. In all cases, the procedure is identical. Firstly the fields at the surface of the emitter are determined. Then the evolution of the effective area as a function of the voltage is calculated using the FN and SN models. Next a WKB calculation is performed across the simulated potential barrier. Finally the field emission current is determined. The main feature is that the curves displace to higher fields as the radii are reduced for this experimentally accessible current range.

For the 1 nm radius tube, F(0) is 7.3 V/nm for 1 pA and 12.3 V/nm for 1 μA. For radii greater than 5 nm, the fields are more typical of conventional FE (respectively, 3.2 and 6.03 V/nm for r = 10 nm). The discrepancy between the curves becomes pronounced at 2 nm and reaches a notable level at 1 and 0.5 nm. For a 0.5 nm radius, currents of 1 pA and 1 μA are obtained for fields of respectively 11.3 V/nm and the extremely high 17.7 V/nm. It is evident that such fields are implausible within the framework of conventional models, as they would correspond to very transparent barriers and unmanageably high emission currents. For the extreme small radii under consideration, the widened tunnel barrier strongly reduces the emission current to acceptable values.

It is interesting to compare these curves with classical pla-

nar models for which $I(E) = J(E) * S$ where the current density, $J(E)$, is a universal curve and S is the emissive surface. Assuming that this emission surface is proportional to the nanotube section ($S \propto r^2$), this means that for the same field, the emitted current by the tube with a radius of 0.5 nm would be 400 times less than that emitted by the tube with a radius of 10 nm. In other words, if the curve for 10 nm is taken as a reference, the $I(E)$ curve for 0.5 nm would correspond to the curve for 10 nm shifted downwards by 2.6 decades. This curve is represented by the dashed black curve in Fig. 2. The very large difference between this curve and the red curve corresponding to 0.5 nm is directly and uniquely due to the widening of the potential barrier.

Additional simulations, not presented here, have been performed with shorter nanotubes, 100 nm, to evaluate eventual shielding by the substrate. These curves superimpose on the curves obtained for a length of 1 μm, showing that the length effect is negligible.

A few comments can be made following these first results:

- The very low values of field proposed during the emission of SWNTs, such as the value of 4.5 V/nm, are unrealistic. For these small radii of curvature, the fields at the surface must be much larger to compensate for the widening of the potential barrier. For example, we have seen that for a nanotube with a radius of 1 nm, there is no emission for a field of 6 V/nm, which is a significant field in classical models. For smaller radii, the necessary fields increase even further.

- Our estimates in Fig. 2 are in good agreement with those of Edgcombe *et al.*[3,26] mentioned above: 13.5 V/nm for 105 nA and a radius of 0.93 nm.

- The simulation package on the GETELEC website[27] was tested, which is a fully open source tool that analyses I(V) data and includes corrections for small radius of curvature emitters[28]. Using our simulated data for a radius of 1 nm, GETELEC found a radius of 1.13 nm, an amplification factor of γ = 2.50 x 10^8 m^{-1}, close to our 3.03 x 10^8 m^{-1}, and an effective area of 7.38 nm^2. These values are in rather good agreement with our parameters, especially given the uncertainties in conventional field emission models.

- The widening of the tunnel barrier also induces other phenomena such as curved Fowler-Nordheim plots or narrower TEDs. More details on these aspects can be found in previous theoretical works on small radii[5–8].

These simulations can also be used to evaluate the differences between nanotubes during growth at a constant applied voltage across the gap. To facilitate comparison with experiments, it is useful to plot the data as a function of voltage rather than electric field. Figure 3 shows the current-voltage characteristics for nanotubes of different radii (length 1 μm in a 2 μm gap). It is again interesting to compare these curves with conventional planar models. Taking the curve for 5 nm as a reference, and considering Edgcombe and Valdré's formula for β and that $S \propto r^2$, we would obtain for a 0.5 nm tube the dashed black curve in Fig. 3. The more than doubling in voltage is the consequence of the wider potential barrier. As the radius is reduced, the necessary applied voltages are still reduced due to the increased β, but not as expected from planar theory.

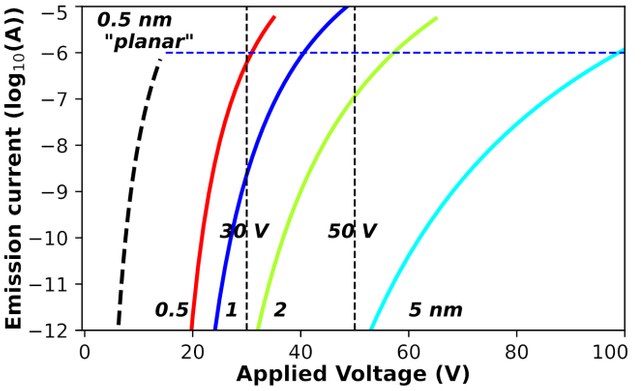

FIG. 3. Simulated current-voltage characteristics for 1 μm long carbon nanotubes with variable radii of 0.5, 1, 2 and 5 nm in a 2 μm gap. Dotted horizontal line corresponds to 1 μA emission current. The vertical dotted lines indicate applied voltages of 30 and 50 V(see text).

These simulations can now be directly applied to our ETEM growth studies. A notable experimental finding was that for a 2 μm gap and a 50 V applied voltage, most nanotubes failed to grow beyond half the gap. (see SM-video1 in Ref.[9]). During the same synthesis the voltage was reduced to 30 V and the nanotubes that subsequently grew were then able to go well beyond this mid-gap, with some approaching the opposite electrode. To compare our simulations with experiment, let us assume that the tubes are destroyed for a current of 1 μA represented in the figure in Fig. 3 by the horizontal blue dotted line. It can be seen in Fig. 3 that for a voltage of 50 V the thinnest nanotubes, 0.5 and 1 nm, should be destroyed even before they reach the middle of the gap. Tubes around 2 nm should reach the middle of the gap and even continue to grow a little before reaching the fixed limit. The largest tubes (around 5 nm) should only start to emit once they reach the middle of the gap and could continue to grow. If the voltage is reduced to 30 V, we can see that the thinnest tubes (0.5 nm) can now reach the middle but hardly exceed it. Tubes with a 1 nm radius located at the midpoint of the gap emit approximately 1 nA and can therefore continue to grow before being destroyed. For nanotubes larger than 2 nm, no further destruction should be observed during growth. Although this model is quite crude with an abrupt limiting current, this analysis seems relatively close to the observations. It would be interesting to confirm that the thinnest nanotubes are indeed those that are destroyed for the shortest lengths during growth under a high electric field.

A final point concerns the changes induced by varying the width of the gap between the two cantilevers. For example, syntheses carried out on samples with a gap of 6 microns are presented below. The relevant parameters are then the width of the gap, g, the applied voltage, V, and the nanotube length, L. Considering $\beta \propto L/r$, the evolution can be qualitatively predicted since one has $F_G = V/g$ and $F = \beta F_G \propto L/rg * V$. For example, for the same applied voltage between cantilevers a 1 micron long tube in a 2 micron gap will emit almost the same current as a 3 micron nanotube in a 6 micron gap. For a

given voltage, the nanotubes (of the same radius) in the middle of the gap emit almost the same current regardless of the width of the gap.

III. FIELD EVAPORATION

The second theme to be discussed is field ion evaporation and in particular what it tells us about the electric fields at small radius nanotube apexes. Note that the pertinent fields are now proposed to be closer to the surface fields F(0). As mentioned previously, carbon nanotubes have the almost unique characteristic of exhibiting an evaporation mechanism in negative polarity (during field emission) and in positive polarity. For FI, we consider the standard model in which the field reduces the activation barrier and evaporation is thermally activated so that the ion yield can be written phenomenologically in the Arrhenius parameterization[29,30]:

$$k = \nu \, exp[-Q(F)/k_b T] \tag{2}$$

where ν ($\nu \approx 10^{13}$ s^{-1}[29,31]) is the "attempt" frequency to overcome the activation barrier, $Q(F)$, which is usually weakly dependent on temperature. It is experimentally observed that $Q(F)$ is given by a monotonic decreasing function of F and

$$Q(F) = Q'_0(1 - \frac{F}{F_e}) \tag{3}$$

where F_e is the evaporation field that corresponds to the field for which the energy barrier vanishes and Q'_0 is related to the bonding energy without an electric field. The total evaporation rate is obtained by summing the different sites likely to be evaporated multiplied by their own evaporation rate. We will consider the number of sites to be relatively small in the case of a nanotube (a few sites at most) and therefore the evaporation rate given by the equation 2 represents the evaporation of the whole nanotube extremity. This model, originally developed for metals, has been widely generalized for the study of semiconductors and insulators[31]. Of course, ambiguities remain for carbon due to its covalent structure, and even more so for nanotubes with their shell-like geometry. For example, do the atoms leave individually or in the form of small clusters? With what charge ? etc. In the following, however, we will use this model as a starting framework, despite its eventual limitations.

The first point therefore concerns the information available in the literature on the various parameters involved in this mechanism. In the following, the most relevant experimental and theoretical work on FI will be critically discussed. A second point concerns the multiplicity of nanotubes and apparatus used in these different studies. Comparing the same nanotubes in the same experiment would give a better understanding of evaporation in both polarisations. This is the objective of the experiments carried out *in situ* in an ETEM presented below.

A. Experimental and theoretical results on nanotube field evaporation

The experimental work carried out on carbon nanotubes in positive polarity (no FE) started with field ion microscopy (FIM) realized on MWNTs[32–36] and SWNTS[37–39]. The samples under investigation were in the form of bundles or aggregates of nanotubes. The majority of observations, when specified, were carried out at low temperatures using helium as imaging gas and for which the field required for Best Image Voltage (BIV) is generally estimated at 45 V/nm. During observations of varying duration with He, the image pattern could also change. For example, Saito *et al.* observed the opening of closed MWNTs during FIM with Helium[32]. It therefore seems that evaporation can occur for these fields and at low temperatures, but at a very low rate. In the same article, once the tube was opened, the tube shortened significantly, which can be interpreted as the fact that the open tube evaporates more easily than the cap of the closed tube.

Few studies have focused specifically on the FI[39–42] of carbon nanotubes. These studies are indeed particularly delicate because there is so little material at the apex and its removal leads to rapid evolution of the extremity and therefore a decrease in the amplification factor. For example, for a (10,10) SWNT with r = 0.678 nm, 100 nm in length corresponds to 16,400 carbon atoms. In the paper by Hata *et al.*[40] they field evaporated MWNTs and SWNTs and they calibrated their field from the field amplification factor extracted from previous I(V)'s which may be debatable[43]. In both cases they observed mainly the evaporation of singly charged carbon clusters C_5^+ and C_{20}^+ with the intensity of C_{20}^+ being prominent. They estimate that evaporation begins for fields of around 10 V/nm and, in a graph (ref.[40], Fig. 4), they report the evolution of the C_{20}^+ peak intensity as a function of the field strength between 10 and 40 V/nm. We are quite skeptical about these values although they are frequently used in the literature. Firstly, the value of 10 V/nm is extremely low and is in contradiction with the FIM observations with He carried out by the same team. Secondly, from the very beginning of evaporation, an increase of a factor of 4 in the applied field (between 10 and 40 V/nm) is substantial and should probably raise F above F_e. It is therefore much more likely that the tubes had shortened significantly during the experiment and that the increase in voltage had only compensated for the drop in the amplification factor or resulted in only a more limited increase in the field at the end of the tubes. Finally, although their experiments are instructive in terms of emitted species, the estimate of their field appears to be highly inaccurate.

Liu and Tsong[41] studied field evaporation of graphite tips using a pulsed-laser time-of-flight atom probe. They also observed that the tip was stable during low temperature He FIM and can withstand fields of about 45 V/nm. By focusing the laser on the tip apex they estimate a temperature rise of over 1000 K and that under a field of about 20-30 V/nm carbon atoms are field evaporated mostly as C^{2+} and C^+.

From a theoretical perspective, Nakaoka *et al.*[44] made *ab initio* studies of FI of thin SWNTs ((5,0), r = 0.196 nm and (7,0), r = 0.274 nm). They evaluated the energy barriers, Q(F),

for some fields and geometries, including open and closed nanotubes. They show that the activation energy barrier from the top of open nanotubes is lower than that of closed nanotubes, which is explained by the different number of C-C bonds. For the emission of a C^+ ion from an open nanotube, they obtain for example for a field strength of 30 V/nm a barrier height of 4.1 eV. We estimate that their values are quite high but they consider themselves that their values are overestimated due to their simulation procedure. These results are discussed in the Discussion section of this article.

Now let us examine the experimental works in negative polarity. Actually, a lot of works reported field evaporation or destruction of carbon nanotubes during FE[1,2,4,45–50]. For SWNTs the emission current for which the evaporation occurs is measured to be roughly between 200 nA and 2 µA and it can be much higher for MWNTs. For the fields at which field evaporation occurs, we have already seen that the estimates are in an extremely wide range. For SWNTs, the simulations presented above are clearly in agreement with the highest estimates of these fields. Finally, in experiments where the temperature increase could be estimated or measured during FI all observed temperature increases were between roughly 1600 K (i.e. SWNT[1]) and more than 2000 K (i.e. MWNT[47]). Of course, the fact that nanotubes are stable at these temperatures (low surface diffusion compared to metals for example) explains the rather unique nature of the observation of FI during field emission.

Theoretical studies on field evaporation in negative polarity are quite rare and often irrelevant. Note however an article from Wu *et al.*[51] that studied field evaporation from a clean graphite plane surface. Interestingly they observe a small difference between positive and negative ions. For example to obtain the same barrier height they calculated necessary fields of 61.6 and 60.5 V/nm for C^+ and C^- respectively and they obtain the same behavior for cluster emission. Even if the difference is quite small this shows that a dissymmetry can exist between the two polarizations.

In summary, the results on FI from nanotubes in the literature are relatively rare and the proposed field values are debatable. However, some aspects seem to be established. In positive polarity and at low temperature, nanotubes can withstand fields of typically 45 V/nm and evaporation can start to occur above these fields. Moreover closed tubes are more difficult to evaporate than open tubes. For field evaporation in negative polarity, the experiments suggest an evaporation mechanism concomitant with significant heating of the nanotube induced by the field emission current, but there is no consensus on the fields at which this evaporation occurs.

B. Field evaporation experiments in ETEM

Syntheses of SWNTs in ETEM were performed in the gaps between two silicon cantilevers[9,10]. A catalyst is first deposited on the cantilevers. Once the sample is inserted into the ETEM, one of the two cantilevers is heated by the Joule effect and the second cantilever is biased with a voltage source to generate the electric field in the gap. For CNT synthesis, acetylene is introduced at a pressure of a few 10^{-4} mbar and the nanotubes are observed to grow across the gap as a result of the orientation of the electric field and force. More details on the growth procedure are provided in previous works[9,10]. HRTEM observations and Raman measurements were regularly carried out after growth to verify that the nanotubes were predominantly SWNTs and to obtain an estimate of the radii. The chirality of the nanotubes is not yet readily available and experiments are underway and will be published elsewhere. Note that Raman analysis gives an average radius of the produced nanotubes of around 0.7 nm.

In previous experiments, almost all of which were carried out at negative polarity, three destruction mechanisms were observed. In the most common one, nanotubes are pulled off the substrate. Note that a significant fraction of these torn off nanotubes (termed nanodarts) form strong connections to the opposite electrode and become realigned by the electric field. A second mechanism is the gradual evaporation of the nanotubes, and a third, more original mechanism begins with the self-oscillation of the nanotube, followed more or less rapidly by the disappearance of the tube. In these new experiments the syntheses have been conducted under either positive or negative polarities and the applied voltage could be varied during or after synthesis. During growth and subsequent experiments, the temperature of the heated cantilever is around 1000 K, which thus corresponds to the temperature of the tubes on the synthesis electrode. In the video, the contrasts obtained for the nanotubes can be bright or dark depending on both the polarization of the cantilevers and the ETEM settings. In the images and videos presented below the settings chosen were such that the nanotubes appear bright in positive polarity (no FE) and dark in negative polarity (possible FE). Note that this choice is the opposite of what was used in previous articles[9,10].

In a first experiment, we carried out two syntheses under the two different polarities following the same procedure. The syntheses were started at high voltage, which was gradually reduced and then increased again in order to observe the field evaporation mechanism. These experiments were realized using 6 μm gap samples. For the synthesis under negative polarity (see SM-video1 of the supplementary material), we observe the growth of numerous nanotubes that become longer and longer as the voltage is gradually reduced. As already observed in previous experiments, many nanotubes are pulled off the substrate by electrostatic forces with the nanotubes disappearing completely. In the video, the synthesis stops at one point due to an interruption in the acetylene supply, but this does not affect the experiment. The voltage decrease is clearly visible in the videos through the reduced contrast of the images of the nanotubes. When the voltage is gradually increased again, we still see tubes being torn off, but also many nanotubes whose length is gradually decreasing. Figure 4 shows several images taken from the video clearly showing the tubes gradually shortening through apex carbon evaporation.

The second synthesis performed in positive polarity corresponds to SM-video2 of the supplementary material. As the voltage decreases, the tubes grow longer and longer and some

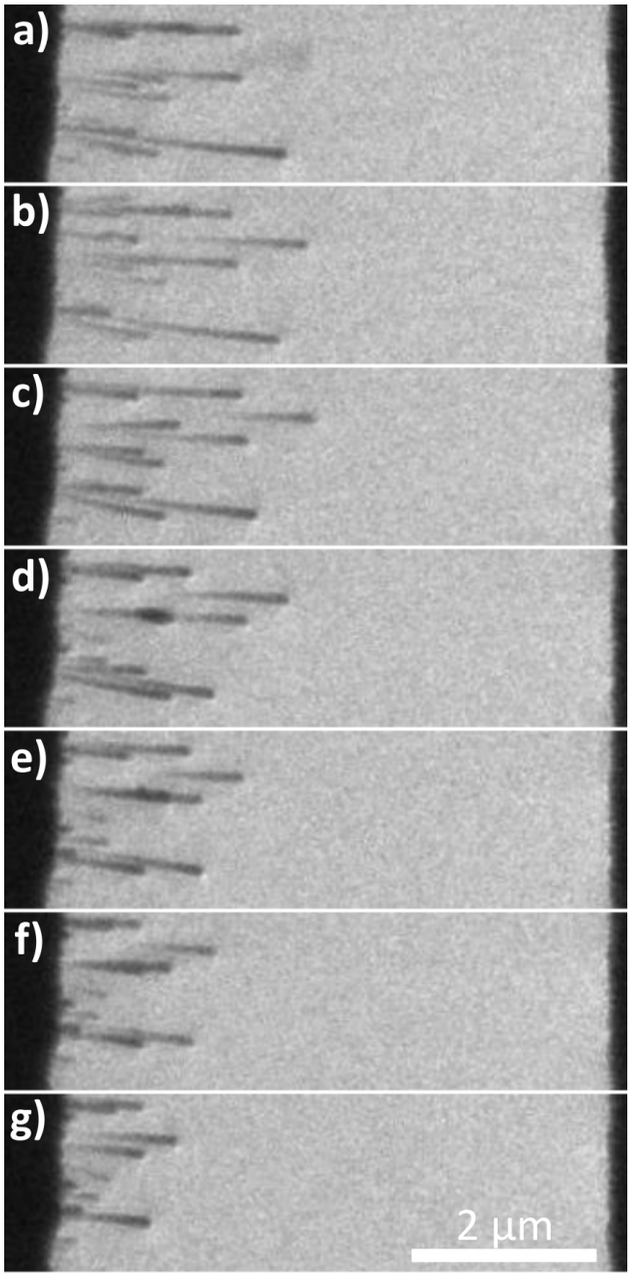

FIG. 4. Images taken from SM-video1 of the supplementary material during the negative polarity experiments. a) to g) Evolution of the nanotubes over time as the voltage is increased. The different nanotubes that gradually evaporate can be clearly seen, as well as some nanotubes that are torn off.

even touch the counter-electrode at the lowest voltage. On the other hand when the voltage is increased, we only see tubes torn from the substrate. There were no nanotubes gradually reducing in length as was the case with negative polarity. We can also see that at the end of the experiment the tubes in negative polarity are much shorter than those in positive polarity. Assuming the same radius distribution for both polarities, the comparison of lengths indicates that for the same field one can

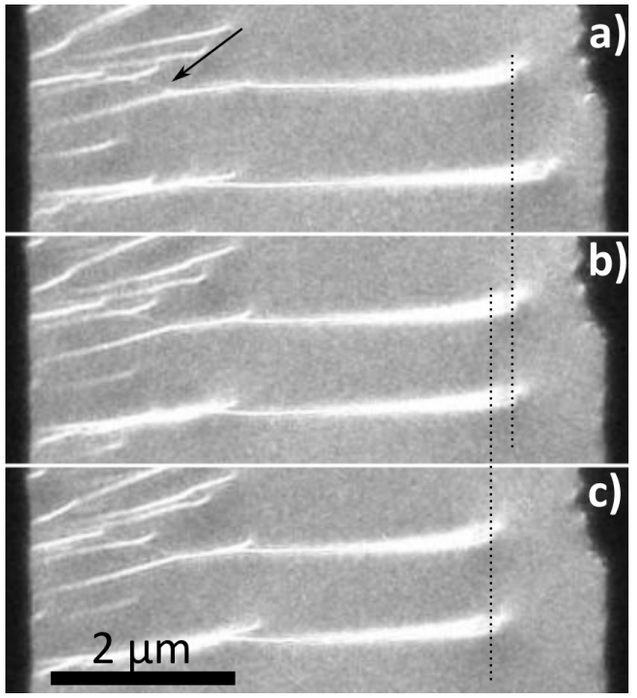

FIG. 5. Example of positive polarity field evaporation. a) Image before evaporation. b) A reduction in the length of the longest nanotube is observed. c) After a further increase in voltage, a simultaneous reduction in the two longest nanotubes is observed. The base of these nanotubes is complex. For example, the upper tube presents a characteristic Y-shape (see the black arrow in a)), indicating that at least one or more other nanotubes are attached to its base.

have evaporation in negative polarity but not in positive one. This observation was confirmed in all our experiments. However, in some very rare cases, evaporation in positive polarity has been clearly observed. An example is presented in Fig. 5 (and see SM-video3 of the supplementary material). Figure 5 a) shows the nanotubes before evaporation. Figure 5 b) shows the longest tube slightly reduced in length and, after a further increase in voltage, Figure 5 c) shows the two nanotubes further reduced in length. However, the structure of these tubes is more complex. A Y-shape (indicated by a black arrow in Fig. 5 a)) can be seen at the base of one nanotube, indicating that the tube is connected to at least one other nanotube. The structure at the base of the longest tube is also complex.

Finally, a last example of the dissymmetry between the two polarities is illustrated in Fig. 6 (and see SM-video4 of the supplementary material). A nanotube in positive polarity (bright) is directly opposite a nanodart, i.e. a nanotube connected to the other electrode[10] (which therefore appears dark) and which can enter into field emission. In this case, the temperature of the left electrode is 1000 K, while the unheated right electrode is about 300 K. Initially, the two tube fragments are almost in contact. As the voltage is increased, the negative-polarity nanotube gradually evaporates, even though it is shorter and connected to the low temperature electrode. The video even shows the tube oscillating a little on its own, confirming that it is in a field emission regime.

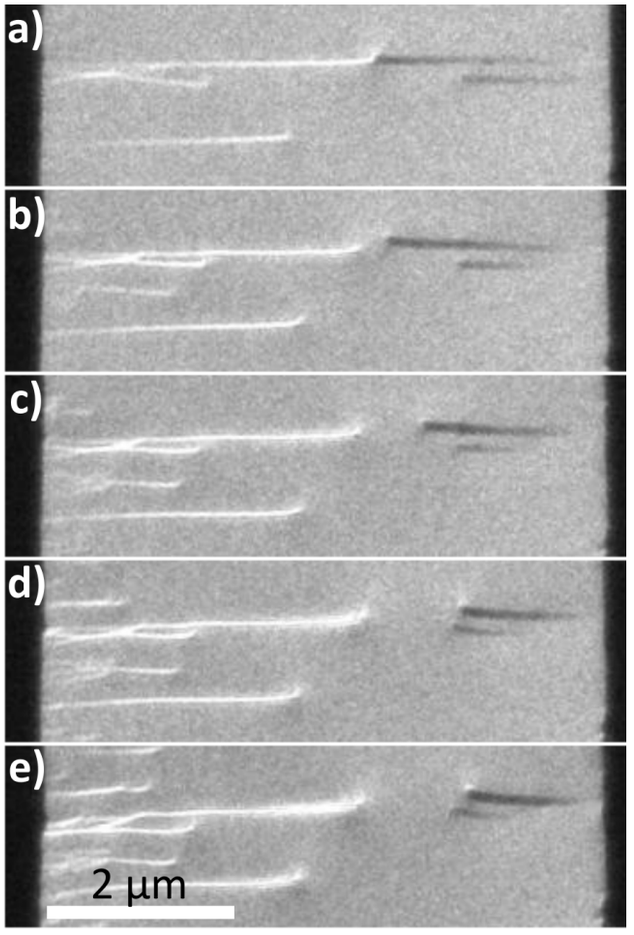

FIG. 6. a) A nanotube in positive polarity, which appears bright and is connected to the growth electrode (1000 K) is directly opposite a nanodart, i.e. a nanotube which appears dark and is connected to the opposite electrode (300 K) and then in negative polarity (FE possible). Initially, the two tube fragments are almost in contact. b) to e) As the voltage is increased, it can clearly be seen that the nanotube in positive polarity is gradually evaporated while the opposite nanotube retains its length.

All these results clearly confirm the dissymmetry between the two polarities. Looking at Eq. 2 the two possible explanations are activation energy barriers, Q(F), that are significantly different for the two polarities or a temperature increase induced by field emission that facilitates evaporation. The first explanation seems unlikely, although small differences can be expected. The most likely explanation, given the already published heating observations, is thermal heating, which seems necessary even for thin SWNTs where large fields are present.

The question remains as to why we observe so little evaporation in positive polarity when fields as large as desired could be obtained for fairly long nanotubes and high applied voltages. This brings us to the question of the electrostatic forces and the mechanical pulling that are associated with these high fields.

Field 10 V/nm	tensile Force (nN)	$stress_1$ (MPa)	$stress_2$ (MPa)
r = 0.5 nm	0.307	391	288
r = 1 nm	1.23	391	575
r = 2 nm	4.91	390	1148
r = 5 nm	30.56	389	1023
r = 10 nm	121.5	387	1221

TABLE I. Simulated forces and stresses on carbon nanotubes with radii of 0.5, 1, 2, 5 and 10 nm for a given electric field at the apex of 10 V/nm. The thin nanotubes are assumed to be SWNTs and for r = 5 nm and r = 10 nm a three wall nanotube and a five wall nanotube are considered respectively where r is the mean radius.

IV. ELECTROSTATIC FORCES AND STRESSES

This section focuses on the electrostatic forces acting on the nanotubes. This is done using the previous simulations which give the field at each point of the hemispherical cap. The electrostatic pressure is then given by $\frac{\varepsilon_0}{2}F^2$ and the total longitudinal tensile force is obtained by summing the longitudinal components of the electrostatic forces over the whole hemisphere. For our previous nanotube (r = 1 nm, L = 1μm and a bias of 20 V), a field of 6.06 V/nm at the apex was obtained and the total calculated pulling force is 0.45 nN.

Tensile stress can then be obtained by dividing the force by the surface. A recurring problem with SWNTs is how to calculate the cross-sectional area of the tube. Two approximations are commonly used. The first simply considers the internal area, πr^2, and the second considers that the thickness of the nanotube wall is t, with generally $t = 0.34$ nm, giving an effective surface area of $\pi((r+t/2)^2-(r-t/2)^2)$. For r = 1 nm it gives respectively surfaces of 3.14 nm^2 and 2.14 nm^2 resulting in slightly different tensile stresses values of 143 MPa and 210 MPa respectively. Note however that the first option scales as r^2 whereas the second scales as r. We next use $stress_1$ and $stress_2$ depending if the inner surface or the annulus area is considered. An obvious feature of nanotubes is that their diameter is constant. This means that the stress is transmitted entirely along the nanotube, at the nanotube/catalyst and possibly at catalyst/substrate interfaces. $Stress_2$ could then correspond to the nanotube/catalyst interface stress if only the external annulus of the nanotube is in contact with the catalyst, and $stress_1$ could be the catalyst/substrate stress if the contact area between the two is of the order of the nanotube radius.

The forces and stresses can be calculated equivalently for nanotubes of different radii. In table I they are given for nanotubes with radii between 0.5 and 10 nm and for the same field strength of 10 V/nm. For the 5 nm and 10 nm nanotubes, we considered respectively a three-wall and a five-wall nanotube, with the radii corresponding to the averaged radius. Since the variation of the mean field is smooth as a function of the radius, we obtain forces that are almost proportional to the surface area of the tube and $stress_1$ is then almost constant whereas $stress_2$ increases as r. For 5 and 10 nm radii, $stress_2$ is limited by the increasing number of walls.

However, the constant field forces do not capture the evolution of these forces as a function of current during field emission. Again, the surface field is no longer the dominant pa-

Current 1 μA	tensile Force (nN)	stress$_1$ (MPa)	stress$_2$ (MPa)
r = 0.5 nm F = 17.66 V/nm	0.958	1220	897
r = 1 nm F = 12.17 V/nm	1.82	579	852
r = 2 nm F = 9.13 V/nm	4.09	325	957
r = 5 nm F = 6.95 V/nm	14.8	188	495
r = 10 nm F = 5.95 V/nm	43	136	431

TABLE II. Simulated forces and stresses on carbon nanotubes with radii of 0.5, 1, 2, 5 and 10 nm for a given emission current of 1 μA. The field required to obtain this current is also indicated. The thin nanotubes are assumed to be SWNTs and for r = 5 nm and r = 10 nm a three wall nanotube and a five wall nanotube are considered respectively where r is the mean radius.

rameter determining the emission current due to the widening of the tunnel barrier. For example, for the same 10 V/nm apex field, the 10 nm tube should emit a current well in excess of 1 μA, whereas a 0.5 nm tube would emit a current of less than 1 pA. To correct for these variations, Table II shows the forces and stresses for the same emission current of 1 μA. It appears that for small radii, the forces evolve approximately proportional to the radius, reducing stress$_1$ but keeping stress$_2$ approximately constant. Thus, for the same current, the thinnest nanotubes are subjected to the greatest stress, as a result of the widening of the tunnel barrier. For larger radii, the fields evolve more and more slowly and we tend to find, as before, a force that varies almost as r^2.

For conventional positive field evaporation and FIM still higher fields are required. Table III presents the fields and stresses for a r = 1 nm tube and fields of 10, 30, 45 and 50 V/nm and high stresses of more than 10 GPa can be obtained. For the nanotube itself such stress is still low. Taking a Young's modulus of 1 TPa, which is a classical value found in the literature, a field of 50 V/nm corresponds to a stress of around 10 GPa or a tensile strain of 1 %. This value is well below the maximum values reported in the literature[52–56]. For individual SWNTs or bundles and fine MWNTs, tensile strengths above 80 GPa have been measured[52] and elongations above 10 % have been obtained[53]. Theoretical calculations give even higher values with fracture stresses above 100 GPa[55] and fracture strains above 30 %[56]. In other words, for good quality nanotubes, the maximum forces and stresses during field emission or evaporation remain well below the maximum values predicted or measured and this explains why so few partial fractures of nanotubes are observed during our synthesis or field emission experiments[9,10].

In our case, to explain the large number of pulled-out nanotubes, it is clear that the fragile zone is located either at the nanotube/catalyst interface or at the catalyst/substrate interface. Note that all the samples discussed in the previous section and analyzed by FIM or evaporation were agglomerates of nanotubes or bundles. In this case, it is likely that the force exerted on the protruding tube or tubes can be spread over an increasing surface area, reducing the stress. This is not

SWNT r = 1 nm	tensile Force (nN)	stress$_1$ (MPa)	stress$_2$ (MPa)
10 V/nm	1.23	391	575
30 V/nm	11.0	3517	5172
45 V/nm	24.87	7914	11640
50 V/nm	30.7	9770	14370

TABLE III. Simulated forces and stresses on carbon nanotube with radius 1 nm for a high electric field of 10, 30, 45 and 50 V/nm.

the case for an individual nanotube. Dedicated simulations and observations at the different interfaces should enable us to clarify this point.

V. DISCUSSION

The first aspect to be discussed in more detail concerns the high fields at the nanotube tips during field emission. It seems necessary to rapidly obtain clear experimental evidence on nanotubes whose radius is well determined. Indirect techniques[3,4] have been used, but a more direct experimental technique that proves the existence of these high fields would be a plus for the study of these small objects. A relatively simple technique to implement could be the FEM / FIM comparison. The parameter of interest here is the ratio between the voltage required for FIM imaging at the Best Image Voltage and the voltage required to obtain a given field emission current (or pattern). For a conventional tungsten tip and helium imaging, a ratio of 9-10 is often quoted. Of course this depends on the reference chosen for the current but if we use for example a field strength of 5 V/nm to obtain an intermediate current and a value of 45 V/nm for the helium BIV, this corresponds to a ratio of 9. For a SWNT with a radius of 1 nm and a current of about 100 nA, a field strength of about 11 V/nm is required according to our simulations. It is only a ratio of 4 compared to the BIV field of 45 V/nm. Such a low value would clearly indicate the presence of a large field at the end of the nanotube. Argon, which has BIV of 18.5 V/nm can also be used. Note, however, that the theory of ion imaging (required field, ionisation distance, etc.) is based on a planar model. For SWNTs, the rapid variation of the electric field could also modify these quantities. However, as these ionisation mechanisms take place at Angstrom distances to the surface, it is likely that the changes will be less significant than for field emission. Another aspect to consider is that sc-SWNTs and m-SWNTs have been assumed to be good metals, which is reasonable given the syntheses and experiments conducted at 1000 K. However, very different behaviour is expected at ambient or low temperatures.

A second point is the very strong dissymmetry observed experimentally between evaporation in positive and negative polarity. As already discussed the most probable explanation is a heating effect induced by the field emission which strongly favors evaporation even for thin nanotubes for which large fields are present at the surface. This, of course, brings us to the question of the heating mechanism and all the related issues, such as determining the current at which the temperature rise becomes significant. Quite a few articles treat the modeling

of these thermal effects on carbon nanotubes with varying degrees of sophistication[57–70]. Note however that if field emission is included in the simulations to obtain I(V,T) evolutions, we have just seen that conventional field emission models are no longer valid and a proper calculation of the actual barrier transmission is required for a more realistic estimation of the current. Finally, to predict current saturation or destruction, a good description of the field evaporation mechanisms and an estimate of the mechanical fractures are required.

A third point concerns electrostatic forces and stresses. Because of the individual growth of our nanotubes, the stress is transferred along the complete tube and at the interface with the catalyst / substrate. This results in many nanotubes being ruptured and in almost all cases we see the complete disappearance of the nanotube, clearly demonstrating that the rupture occurs at the level of the catalyst/substrate. It is clear from the videos that this rupture is the main destruction mechanism for our nanotubes. In positive polarity, the cases where evaporation can be observed generally correspond to nanotubes adhering to other nanotubes or forming characteristic Y structures as in Fig. 5. In this case, it is likely that these contacts distribute the stress so that evaporation can be observed.

These aspects are important from an application point of view to improve cathodes in terms of current or current density. For example, the EFDS technique we used allows the growth of many individual and oriented SWNTs, which can be interesting for increasing the emitter density. One potential disadvantage might be that for our current growth and catalyst protocol, these nanotubes directly connected to the substrate appear more fragile, both mechanically and perhaps also thermally. The growth of entangled nanotube mats by CVD or the realization of cathodes from entangled SWNTs from nanotube papers[71] logically will have much lower emitter densities, but these emitters (the protruding nanotubes) are surely mechanically more robust and allow better heat dissipation. Improving SWNT cathodes therefore requires either improving the mechanical anchoring of individual nanotubes or finding the best compromise between different ways of increasing emitter density while maintaining good mechanical and thermal resistance. Cathode optimisation will also pass by post growth treatments for which these observations of field induced destruction on individual nanotubes will be of considerable aide.

Finally, to summarize our observations, we present a scenario based on a simple model that nevertheless captures the qualitative evolution of the observed phenomena. Starting from Eqs. 2 and 3 let us assume that all nanotubes (open or closed, SWNT or MWNT, positive or negative polarity) have a unique activation energy barrier, $Q(F)$. Assuming that equation 3 is valid over the whole field range (which is probably not the case) and as this function is linear, only two points are necessary to determine $Q(F)$ completely. Let us take a first point corresponding to an evaporation rate of k = 0.01 s^{-1} for a field of 45 V/nm at 100 K, which roughly corresponds to the fact that at low temperature He FIM nanotubes can open, giving a barrier height of 0.3 eV. Next, let us consider Liu and Tsong's estimate and take k = 100 s^{-1} for a field of 32 V/nm at 1000 K. This gives a barrier height of 2.19 eV. Q_0 = 6.83 eV and F_e = 47 V/nm are then obtained. Again, this is a qualitative approach and these values are just first order estimates. From these values we can then estimate the temperature (at a given field strength) or the field strength required (at a given temperature) to obtain a fixed evaporation rate.

During electron emission, fields ranging from 7-8 V/nm for large nanotubes to 17-18 V/nm for the thinnest were required for currents in the μA range. Assuming no temperature rise due to the emission current, nanotubes attached to the growth electrode are at 1000 K. In this case, no evaporation is possible. Even for thin tubes, for 1000 K and a field F = 18 V/nm we get k < $10^{-8} s^{-1}$ i.e. no evaporation in pratice.

An evaporation rate close to 1 s^{-1} for 18 V/nm requires temperatures of around 1650 K at the apex of the nanotube, which clearly shows the need for additional heating. However, for these temperatures, field evaporation of the largest nanotubes is still impossible. For a field strength of 8 V/nm, an evaporation rate of 1 s^{-1} is obtained for a temperature of 2200 K. This would indicate that the thinnest tubes would evaporate at lower temperatures than the larger nanotubes, but would still require Joule heating during field emission. The range of temperatures obtained is consistent with the values measured or estimated in the experiments.

In positive polarity, and therefore without any heating mechanism, the temperature of the nanotubes is 1000 K. The field strength required at this temperature to obtain an evaporation rate of 1 s^{-1} must then be greater than 29 V/nm. If the interfaces cannot withstand forces and stresses greater than those corresponding to, say, 25 V/nm, the nanotubes would be torn off before evaporation could be observed.

A question is what would change if the electrode temperature were at room temperature instead of 1000 K. For negative field evaporation, a higher current is expected to induce a higher temperature rise. However, it is likely that the field and temperature values will change relatively little. In fact, if the field emission current is such that it causes a temperature rise of 600 K, it does not take much more current to reach 1300 K[57], so that the field increase is relatively small. If the field changes very little, the temperature required for evaporation will also change very little and the values should remain more or less the same (considering that nanotubes continue to behave as good metals. At 300 K a very different behaviour is expected for sc-SWNTs). However, for positive polarity field evaporation the effect should be much greater. At 300 K the field strength required for evaporation is 41.7 V/nm. This higher field corresponds to higher stresses and better mechanical contact is required to achieve this value.

In a previous section we saw that Nakaoka *et al.*[44] had calculated an activation energy barrier of 4.1 eV for the departure of an C^+ ion from an open (7,0) nanotube at a field of 30 V/nm. We considered previously this value to be slightly too high compared to experiments. In fact, for 1600 K, evaporation should start for fields greater than 30 V/nm that are incompatible with field emission (transparent barrier). However, their approach to theoretically simulate the energy barrier as a function of the field is extremely interesting. By correcting the overestimation they attribute to the fact that their tube is charged in their simulation when the ion leaves, they could provide Q(F) evolution functions for any nanotube,

open or closed. These curves are important for efficiently simulating field evaporation during field emission.

Although relatively crude, this approach successfully reproduces the main features of our observations on nanotube evaporation under both positive and negative polarity. We hope that new experimental or theoretical results could rapidly refine this model.

VI. CONCLUSION

To conclude, simulations and experimental results on the specificities of SWNTs at high fields and during field evaporation were presented. Due to the nanometric radii of curvature, very intense electric fields are required for field emission, e.g. up to 17 V/nm for a radius of 0.5 nm and a current of 1 μA. Experimental observations on the same nanotubes show a strong dissymmetry between the evaporation in positive and negative polarity that prove that a heating mechanism induced by the field emission current is necessary even for the thinnest nanotube. These high fields are obviously accompanied by high mechanical stresses that lead to numerous rupture at the catalyst/substrate level. Finally, a first attempt is made to gather the experimental data and integrate them into the field evaporation domain (and equations). Although there is clearly room for improvement, this allows us to obtain a scenario that is consistent with the experimental observations. Although many of the points addressed here have already been studied in the literature, the results were sometimes contradictory or anomalous, and in any case fragmented. In this article, the objective was to bring together in a coherent and quantified way all the aspects related to SWNTs under strong field conditions and evaporation, in order to obtain a better overall view of the problem. This constitutes a necessary step to enable the field emission and field evaporation communities to better identify the many points that still need to be clarified for a better understanding of nanotubes.

VII. SUPPLEMENTARY MATERIAL

See supplementary material for presentation of four videos to complement the article.

ACKNOWLEDGMENTS

Authors acknowledge financial support from the French state managed by the National Research Agency through the projects Solitube (ANR-22-CE09-0005), OFELIA (ANR-21-CE24-0007), NanoMAX (ANR-10-EQPX-50) and 3DX ONline (ANR-15-CE08-0002). The authors acknowledge financial support from the CNRS-CEA 'METSA' network (FR CNRS 3507) for access to the CIMEX platform at École Polytechnique, and gratefully thank the Plateforme Nanofils et Nanotubes Lyonnaise at Claude Bernard Lyon 1 University.

AUTHOR DECLARATIONS

Conflict of Interest

The authors have no conflicts to disclose.

DATA AVAILABILITY

The data that support the findings of this study are available from the corresponding authors upon reasonable request.

[1] K. Dean, T. Burgin, and B. Chalamala, "Evaporation of carbon nanotubes during electron field emission," Appl. Phys. Lett. **79**, 1873 (2001).
[2] Y. Saito, K. Seko, and K. J.I, "Dynamic behavior of carbon nanotube field emitters observed by in situ transmission electron microscopy," Diamond and Related Materials **14**, 1843 (2005).
[3] C. Edgcombe and N. de Jonge, "Deduction of work function of carbon nanotube field emitter by use of curved-surface theory," J. Phys. D: Appl. Phys. **40**, 4123–4128 (2007).
[4] A. Pascale-Hamri, S. Perisanu, S. Derouet, C. Journet, P. Vincent, A. Ayari, and S. Purcell, "Ultrashort single-wall carbon nanotubes reveal field-emission coulomb blockade and highest electron-source brightness," Phys. Rev. Lett. **112**, 126805 (2014).
[5] J. He, P. H. Cutler, and N. M. Miskovsky, "Generalization of fowler–nordheim field emission theory for nonplanar metal emitters," Applied Physics Letters **59**, 1644–1646 (1991).
[6] A. Kyritsakis and J. Xanthakis, "Derivation of a generalized fowler–nordheim equation for nanoscopic field-emitters," Proceedings of the Royal Society A: Mathematical, Physical and Engineering Sciences **471**, 20140811 (2015).
[7] D. Biswas, R. Ramachandran, and G. Singh, "The tunneling potential for field emission from nanotips," Physics of Plasmas **25**, 013113 (2018).
[8] D. Biswas and R. Ramachandran, "Curvature correction to the field emission current," J. Vac. Sci. Technol. B **37**, 021801 (2019).
[9] P. Vincent, F. Panciera, I. Florea, N. Blanchard, C. Cojocaru, M. Ezzedine, H. Taoum, S. Perisanu, P. de Laharpe, A. Ayari, J. Chaste, K. Saidov, U. Mirsaidov, S. Purcell, and P. Legagneux, "Observations of the synthesis of straight single wall carbon nanotubes directed by electric fields in an environmental transmission electron microscope," Carbon **213**, 118272 (2023).
[10] P. Vincent, F. Panciera, I. Florea, A. Ayari, S. Perisanu, C. Cojocaru, H. Taoum, C. Wei, K. Saidov, U. Mirsaidov, I. Aguili, N. Blanchard, P. Legagneux, and S. Purcell, "Field emission characterization of field aligned carbon nanotubes synthesized in an environmental transmission electron microscope," J. Vac. Sci. Technol. B **42**, 022802 (2024).
[11] S. Masur, C. Edgecombe, and C. Barnes, "On modeling the induced charge in density-functional calculations for field emitters," J. Vac. Sci. Technol. B **40**, 042802 (2022).
[12] B. Lepetit, "A quantum mechanical model of field emission from a graphene blade type material," J. Appl. Phys. **133**, 135104 (2023).
[13] C. de Castro, T. de Assis, R. Rivelino, F. de B. Mota, C. de Castilho, and R. Forbes, "Restoring observed classical behavior of the carbon nanotube field emission enhancement factor from the electronic structure," J. Phys. Chem. C **123**, 5144 (2019).
[14] C. de Castro, T. de Assis, R. Rivelino, F. de B. Mota, C. de Castilho, and R. Forbes, "On the quantum mechanics of how an ideal carbon nanotube field emitter can exhibit a constant field enhancement factor," J. Appl. Phys. **126**, 204302 (2019).
[15] C. de Castro, T. de Assis, R. Rivelino, F. de B. Mota, C. de Castilho, and R. Forbes, "Modeling the field emission enhancement factor for capped carbon nanotubes using the induced electron density," J. Chem. Inf. Model. **60**, 714 (2020).
[16] C. de Castro, T. de Assis, R. Rivelino, F. de B. Mota, and C. de Castilho, "Using static linear response theory to describe field emission enhancement and a field-induced insulator-conductor transition," J. Vac. Sci. Technol. B **30**, 060601 (2021).
[17] C. Edgecombe and U. Valdré, "Microscopy and computational modelling to elucidate the enhancement factor for field electron emitters," Journal of Microscopy **203**, 188 (2001).
[18] R. G. Forbes, C. Edgecombe, and U. Valdre, "Some comments on models for field enhancement," Ultramicroscopy **95**, 57–65 (2003).

[19]W. Dyke and W. Dolan, "Field emission," in Advances in Electronics and Electron Physics, Vol. 8 (Elsevier, New york, 1956) pp. 89–185, $j = \frac{aF^2}{\phi} exp(-\frac{b\phi^{3/2}}{F})$ for a triangular barrier, a = 1.54 10^{-6} and b = 6.83 10^7.
[20]E. Murphy and R. Good, "Thermoionic emission, field emission and the transition region," Phys. Rev. **102**, 1464 (1956), $j = \frac{aF^2}{\phi} exp(-\frac{bv(y_0)\phi^{3/2}}{F})$ where y and description of v as a combination of elliptic integrals are given in the paper.
[21]H. Ago, T. Kugler, F. Cacialli, W. Salaneck, M. Shaffer, A. Windle, and R. Friend, "Work functions and surface functional groups of multiwall carbon nanotubes," J. Phys. Chem. B **103**, 8116 (1999).
[22]S. Suzuki, C. Bower, Y. Watanabe, and O. Zhou, "Work functions and valence band states of pristine an cs-intercalated single-walled carbon nanotube bundles," Appl. Phys. Lett. **76**, 4007 (2000).
[23]M. Shiraishi and M. Ata, "Work function of carbon nanotubes," Carbon **39**, 1913 (2001).
[24]P. Liu, Q. Sun, F. Zhu, K. Liu, K. Jiang, L. L., Q. Li, and S. Fan, "Measuring the work function of carbon nanotubes with thermionic method," Nano Letters **8**, 647 (2007).
[25]S. Purcell, P. Vincent, S. Perisanu, A. Ayari, and P. Poncharal, "Field emission from the edges of single-layer graphene," in Nanostructured carbon electron emitters and their applications (Jenny Stanford Publisihing, 2022).
[26]N. de Jonge, M. Allioux, J. Oostveen, K. Teo, and W. Milne, "Low noise and stable emission from carbon nanotube electron sources," Applied Physics Letters **87**, 133118 (2005).
[27]See www.getelec.org.
[28]A. Kyritsakis and F. Djurabekova, "A general computational method for electron emission and thermal effect in field emitting nanotips," Comput. Mat. Sci. **128**, 15 (2017).
[29]M. K. Miller and R. G. Forbes, "Atom-probe tomography. the local electrode atom probe," (Springer, 2014).
[30]W. Lefebvre-Ulrikson, F. Vurpillot, and X. Sauvage, "Atom probe tomography: Put theory into practice," (Academic Press, 2016).
[31]M. Karahka and H. Kreuzer, "Kinetics of silicon field evaporation," Materials Characterization **146**, 319 (2018).
[32]Y. Saito, M. R., and H. K., "Field ion microscopy of multiwall carbon nanotubes : observation of pentagons and cap breakage under high electric field," Surface Science **499**, L119–L123 (2002).
[33]V. Ksenofontov, V. Gurin, I. Gurin, V. Kolosenko, I. Mikhailovskij, E. Sadanov, T. Mazilova, and O. Velikodnaya, "Low-temperature field ion microscopy of carbon nanotubes," Low Temp. Phys. **33**, 858 (2007).
[34]T. Kuzumaki, Y. Takamura, H. Ichinose, and Y. Horike, "Structural change at the carbon-nanotube tip by field emission," Appl. Phys. Lett. **78**, 3699 (2001).
[35]C. Oshima, K. Matsuda, T. Kona, Y. Mogami, M. Komaki, Y. Murata, T. Yamashita, Y. Saito, K. Hata, and A. Takakura, "Electron emission sites on carbon nanotubes and the energy spectra," Jpn J. Appl. Phys. **40**, 1257 (2001).
[36]Y. Saito, K. Hata, A. Takakura, J. Yotani, and S. Uemura, "Field emission of carbon nanotubes and its application as electron sources of ultra-high luminance and light-source devices," Physica B **323**, 30–37 (2002).
[37]D. Lovall, M. Buss, E. Graugnard, R. Andres, and R. Reifenberger, "Electron emission and structural characterization of a rope of single-walled carbon nanotubes," Phys. Rev. B **61**, 5683 (2000).
[38]Z. Zhang, G. Zhang, M. Du, X. Jin, S. Hou, J. Sun, Z. Gu, X. Zhao, W. Liu, J. Wu, and Z. Xue, "Field-ion microscopy observation of single-walled carbon nanotubes," Chinese Physics **11**, 804 (2002).
[39]N. Ohmae, N. Matsumoto, T. Ohata, and H. Kinoshita, "Atomic structure and field evaporation of carbon nanotube studied by atom probe field ion microscopy," Diamond and Related Materials **16**, 1179 (2007).
[40]K. Hata, M. Ariff, K. Tohji, and Y. Saito, "Selective formation of c20 cluster ions by field evaporation from carbon nanotubes," Chem. Phys. Lett. **308**, 343 (1999).
[41]J. Liu and T. Tsong, "Kinetic-energy and mass analysis of carbon cluster ions in pulsed laser stimulated field evaporation," Phys. Rev. B **38**, 8490 (1988).
[42]M. Raghuwanshi, O. Cojocaru-Miredin, and M. Wuttig, "Investigating bond rupture in resonantly bonded solids by field evaporation of carbon nanotubes," Nano Letters **20**, 116 (2020).
[43]A. Ayari, P. Vincent, S. Perisanu, P. Poncharal, and S. Purcell, "All field emission experiments are noisy, … are any meaningful?" J.Vac. Sci. Technol. B **41**, 024001 (2023).
[44]N. Nakaoka and K. Watanabe, "Ab inition study of field evaporation from single-walled carbon nanotubes," Phys. Rev. B **65**, 155424 (2002).
[45]A. Rinzler, J. Hafner, P. Nikolaev, L. Lou, S. Kim, D. Tomanek, P. Nordlander, D. Colbert, and R. Smalley, "Unraveling nanotubes : Field emission from a atomic wire," Science **269**, 1550 (1995).
[46]A. Umnov and V. Mordkovich, "Field-induced evaporation of carbon nanotubes," Applied Physics A **73**, 301–304 (2001).
[47]S. Purcell, P. Vincent, J. C., and V. Binh, "Hot nanotubes: Stable heating of individual multiwall carbon nanotubes to 2000 k induced by the field-emission current," Phys. Rev. Lett. **88**, 105502 (2002).
[48]J. Bonard, K. C., K. Dean, and B. Coll, "Degradation and failure of carbon nanotube field emitters," Phys. Rev. B **67**, 115406 (2003).
[49]Z. Wang, R. Gao, W. de Heer, and P. Poncharal, "In situ imaging of field emission from individual carbon nanotubes and their structural damage," Appl. Phys. Lett. **80**, 856 (2002).
[50]M. Wang, Q. Chen, and P. L.M., "Field-emission characteristics of individual carbon nanotubes with a conical tip: The validity of the fowler–nordheim theory and maximum emission current," Small **4**, 1907 (2008).
[51]X. Wu and E. Wolf, "Predicted carbon cluster field evaporation from graphite by pulse-field stm," Surface Science **366**, 353 (1996).
[52]Y. Bai, Z. R., X. Ye, Z. Zhu, H. Xie, B. Shen, D. Cai, B. Liu, C. Zhang, Z. Jia, Z. S., X. Li, and F. Wei, "Carbon naotube bundles with tensile strength over 80 gpa," Nature Nanotechnology **13**, 589 (2018).
[53]Y. Bai, H. Yue, J. Wang, B. Shen, S. Sun, S. Wang, H. Wang, X. Li, Z. Xu, R. Zhang, and F. Wei, "Super-durable ultralong carbon nanotubes," Science **369**, 1104 (2020).
[54]M.-F. Yu, O. Lourie, M. Dyer, K. Moloni, T. Kelly, and R. Ruoff, "Strength and breaking mechanism of multiwalled carbon nanotubes under tensile load," Science **287**, 637 (2000).
[55]Y. Guo and W. Guo, "Mechanical and electrostatic properties of carbon nanotubes under tensile loading and electric field," J. of Phys. D : Appl. Phys. **236**, 805 (2003).
[56]B. Yakobson, M. Campbell, C. Brabec, and J. Bernholc, "High strain rate fracture and c-chain unraveling in carbon nanotubes," Comput. Mat. Science **8**, 341 (1997).
[57]P. Vincent, S. T. Purcell, C. Journet, and V. T. Binh, "Modelization of resistive heating of carbon nanotubes during field emission," Phys. Rev. B **66**, 075406 (2002).
[58]N. Huang, J. She, J. Chen, S. Deng, N. Xu, H. Bishop, S. Huq, L. Wang, D. Zhong, E. Wang, and D. Chen, "Mechanism responsible for initiating carbon nanotube vacuum breakdown," Phys. Rev. Lett. **93**, 075501 (2004).
[59]M. Sveningsson, K. Hansen, K. Svensson, E. Olsson, and E. Campbell, "Quantifying temperature-enhanced electron field emission from individual carbon nanotubes," Phys. Rev. B **72**, 085429 (2005).
[60]G. Bocharov and A. Eletskii, "Thermal instability of field emission from carbon nanotubes," Tech. Phys. **52**, 498 (2007).
[61]W. Wei, Y. Liu, Y. Wei, K. Jiang, L.-M. Peng, and S. Fan, "Tip cooling effect and failure mechanism of field-emitting carbon nanotubes," Nanoletters **7**, 64 (2007).
[62]M. Dionne, S. Coulombe, and J.-L. Meunier, "Energy exchange during electron emission from carbon nanotubes: Considerations on tip cooling effect and destruction of the emitter," Phys. Rev. B **80**, 085429 (2009).
[63]S. Purcell, P. Vincent, and A. Ayari, "Heat generation and losses in carbon nanotubes durig field emission," in Carbon nanotube and related field emitters, edited by Y. Saito (Wiley-VCH, 2010) Chap. 7, p. 81.
[64]T. ragab and C. Basaran, "Semi-classical transport for predicting joule heating in carbon nanotubes," Phys. Lett. A **374**, 2475 (2010).
[65]H. Ma, L. Pan, Q. Zhao, Z. Zhao, and J. Qiu, "Thermal conductivity of a single carbon nanocoil measured by field-emission induced thermal radiation," Carbon **50**, 778 (2012).
[66]F. Antoulinakis, D. Chernin, P. Zhang, and Y. Lau, "Effects of temperature dependence of electrical and thermal conductivities on the joule heating of a one dimensional conductor," J. Appl. Phys. **120**, 135105 (2016).
[67]M. Cahay, W. Zhu, S. Fairchild, P. Murray, T. Back, and G. Gruen, "Mul-

tiscale model of heat dissipation mechanisms during field emission from carbon nanotube fibers," Appl. Phys. Lett. **108**, 033110 (2016).
[68]G. Tripathi, J. Ludwick, M. Cahay, and K. L. Jensen, "Spatial dependence of the temperature profile along a carbon nanotube during thermal-field emission," J. Appl. Phys. **128**, 025107 (2020).
[69]D. Mofakhami, B. Seznec, T. Minea, R. Landfried, P. Testé, and P. Dessante, "Unveiling the nottingham inversion instability during the thermo-field emission from refractory metal micro-protrusions," Scientific Reports **11**, 15182 (2021).
[70]J. Ludwick, N. Hernandez, G. Tripathi, M. Cahay, T. Back, and K. L. Jensen, "Influence of thermal contact resistance on the field emission characteristics of a carbon nanotube," J. Vac. Sci. Technol. B **40**, 042804 (2022).
[71]J. Han, S. Lee, H. Go, S. Kim, J. Noh, and C. Lee, "High-performance cold cathode x-ray tubes using a carbon nanotube field electron emitter," ACS Nano **16**, 10231 (2022).